UNDERSTANDING AND OPTIMIZATION OF GAS SENSORS BASED ON METAL OXIDE SEMICONDUCTORS

by

XIAOHUA DU

M.S., Chemical Engineering, Tsinghua University, China, 1999
B.S., Chemical Engineering, Tsinghua University, China, 1996

PREVIEW

A thesis submitted to the
Faculty of the Graduate School of the
University of Colorado in partial fulfillment
of the requirement for the degree of
Doctor of Philosophy
Department of Chemical and Biological Engineering
2007

UMI Number: 3284441

PREVIEW

UMI®

UMI Microform 3284441

Copyright 2008 by ProQuest Information and Learning Company.
All rights reserved. This microform edition is protected against
unauthorized copying under Title 17, United States Code.

ProQuest Information and Learning Company
300 North Zeeb Road
P.O. Box 1346
Ann Arbor, MI 48106-1346

This thesis entitled:

Understanding and Optimization of Gas Sensors Based on Metal Oxide Semiconductors

written by Xiaohua Du

has been approved for the Department of Chemical and Biological Engineering

____

Steven M. George

____

Alan Weimer

____

Date

The final copy of this thesis has been examined by the signatories, and we find that both the content and the form meet acceptable presentation standards of scholarly work in the above mentioned discipline.

PREVIEW

Du, Xiaohua (Ph.D., Chemical and Biological Engineering)

Understanding and Optimization of Gas Sensors Based on Metal Oxide Semiconductors

Thesis directed by Professors Steven M. George

Abstract

Solid-state sensors are one of the most effective tools for detecting toxic and combustible gases, and semiconducting tin oxide is the most widely used material. However, present understanding of the mechanism of gas detection is still immature, and disadvantages such as lack of reproducibility and insufficient sensitivity are frequently observed. This research is aimed at understanding the sensing mechanism of metal oxide semiconductor based gas sensors fabricated by atomic layer deposition (ALD) techniques, and exploring the ways to optimize their sensing performance.

The ALD of tin oxide thin films has been examined using in situ quartz crystal microbalance (QCM) and Fourier transform infrared (FTIR) techniques. The SnO_x films were deposited using sequential exposures of $SnCl_4$ and H_2O_2 at temperatures from 150-430ºC. The linear growth of the tin oxide ALD films was observed by both the mass gain during QCM measurements and the background infrared absorbance increase during FTIR investigations. A growth rate of ~0.7 Å/cycle at 325 ºC was achieved assuming a density of 6.9 g cm^{-3}. Additional ex situ surface analysis such as X-ray photoelectron spectroscopy (XPS), Auger electron spectroscopy (AES), X-ray diffraction and Atomic force microscope (AFM) results revealed that the SnO_x ALD films deposited on Silicon wafers were sub-stoichiometry tetragonal phase polycrystalline SnO_2 with very smooth surface.

The gas sensing process of O_2 and CO on ultra thin tin oxide ALD films

PREVIEW

were studied by in situ FTIR and electrical measurements. Under oxygen, the background absorbance decreases which is consistent with resistivity increase, the sensing process is slow and may be companied with diffusion process; under CO, the background absorbance increases which is consistent with resistivity decrease, whereas the process is quick compared with the oxygen process, showing it is not a complete reverse process of oxygen response. It is also shown that oxygen is not necessary for CO sensing process. The temperature shows a complicated effect on the response of ultra thin SnO_2 gas sensors to O_2 and CO gases.

The thickness effect sensitivity was studied using hotplate prototype gas sensor. The sensitive films with various thicknesses were deposited on the hotplate and the gas sensing experiemnts were conducted under various CO and O_2 concertrations. The highest sensitivity was obtained when film thickness is around 25 angstrom, which is the Debye length. When the thickness of the sensitive film exceeds the Debye length, the resistance of the underlayer plays a important role in the sensitivity and it is hardly influenced by the sensing process which occurs on the surface; When the thickness of the sensitive film is less than the Debye length, the whole film will be influenced by the surface gas sensing processes. A mathematic model describes the effect of film thickness on sensitivity. The model shows consistance with the experiment results for sensitive films with thickness exceeds the Debye length.

PREVIEW

ACKNOWLEDGMENTS

Graduate school is a great life experience that I will memorize forever. I have had the unconditional support from many friends and colleagues.

I would like to begin by thanking the people who made this thesis possible. My best decision in graduate school has to be choosing Prof. Steven George as my advisor. Steve provided the independence and funding for me to accomplish this work. I developed many skills in the challenging environment in George's lab. Steve also provided intellectual guidance, creative freedom and friendship that has made my aboard graduate school experience very rewarding. I would like to thank all of the George Group members both present and past for their help. So, thanks to Yijun Du, Rikard Wind, Robert Grubbs, Noel Rocklein, Jarod McCormick, Markus Groner, Francois Fabrequette, Cari Herrmann, Zachary Sechrist, Arrelaine Dameron, Beau Burton, Christopher Wilson, David Goldstein, Andrew Cavanagh, Nicole Adamczyk, Dragos Seghete. They are really good colleagues and great friends.

I also wish to thank my doctoral thesis committee for their advice and for serving to referee this dissertation. I would like to thank the staffs in chemical engineering office and chemistry office for their help over the years.

In addition to the professional support, numerous friends encouraged and supported me personally. Special thanks go to Junhao Ge, Hui Lu, Mei Hong, Xinhua Liang, Mao Yu and Hanli Liu. They are the ones that made my life full of smile and laugh through the years I have been in Boulder.

Finally, my greatest thanks go to my loving family. I would like to thank my parents, Fengmin and Xiuqin, for their love, their encouragement and the sacrifices they have made for me in the road toward my PhD in the United States.

PREVIEW

I would like to thank my wife, Ziyuan, for always being supportive; I would also thank my son Joshua for being an inspiration. It is to these people that I dedicate this work; I could not have done this without the unwavering support and love that these people generously have given me over the years.

This work was supported by grants from the National Science Foundation (CHE-0408554). I am also thankful for fellowships from the U.S. Department of Education Graduate Assistantships in Areas of National Need (GAANN) program and the University of Colorado.

PREVIEW

Table of Contents

Title Page i

Signature Page ii

Abstract iii

Acknowledgments v

Table of Contents vii

List of Tables xi

List of Figures xii

Chapter 1 Introduction and Literature Review 1

1.1 Overview of Gas Sensors.. 1

1.2 Overview of Solid State Gas Sensors 2

1.3 Tin Oxide Based Metal Oxide Semiconductor (MOS) Gas Sensors...... 5

1.3.1 Crystal Structure and Properties of Tin Oxide........................ 5

1.3.2 History of Tin Oxide Based Gas Sensors............................... 8

1.3.3 Operation Principles of MOS Gas Detectors 13

1.4 Atomic Layer Deposition 24

1.4.1 Basic Concepts of Atomic Layer Deposition 24

1.4.2 Techniques for Studying Atomic Layer Deposition 29

1.4.3 Atomic Layer Deposition of Tin Oxide 34

1.5 Statement of Purpose 36

1.6 References 38

Chapter 2 Experimental Setups.. 51

2.1 Viscous Flow ALD Reactor with In-situ Capabilities...................... 51

2.2 Quartz Crystal Microbalance 54

PREVIEW

2.2.1 Instrument……………………………………………………………… 54

2.2.2 New Sensor Preparation and Epoxy Cure ………………………. 54

2.3 Transmission Fourier Transform Infrared Spectroscopy ……….………. 55

2.3.1 Instrument……………………………………………………………… 55

2.3.2 Preparation of High Surface Area Samples ………………………. 56

2.3.3 Sample Mounting ……………….……………………………………. 57

2.4 Ex situ Analysis ………………………………………………......…….. 59

2.5 References ………………………………..……………………… 60

Chapter 3 In situ Examination of Tin Oxide Atomic Layer Deposition Using Quartz Crystal Microbalance and Fourier Transmission Infrared Techniques …………………..……………………………...61

3.1 Selection of Precursors for SnO_2 ALD………………………….…..…… 62

3.2 In Situ Study by QCM…………………………………………………… 65

3.2.1 Experimental Details ……………..………………………………… 65

3.2.2 Linear Growth of SnO_2 Thin Films by ALD and Self-limiting Surface Reactions …..………………………….…………………. 67

3.2.3 Surface Chemistry for SnO_2 ALD ……………………………… 72

3.2.4 Temperature Influence on SnO_2 ALD …………………………… 76

3.3 In Situ Study of SnO_2 ALD by FTIR………………………………….. 79

3.3.1 Experimental Procedure …….…………………………...…… 79

3.3.2 Surface Chemistry during Half-reactions……..……………………. 80

3.3.3 Linear Growth Observed by FTIR …..…………………………. 85

3.4 Ex-situ Analysis of SnO_2 Thin Films Grown by ALD ……………….. 93

3.4.1 X-ray Diffraction …….……………….………………………… 94

PREVIEW

3.4.2 X-ray Reflectivity ……………………………………………………… 98

3.4.3 AES and XPS ………………………………………………………… 100

3.4.4 Four-point Probe ……………………………………………………… 104

3.4.5 AFM …………………………………………………………………… 107

3.5 Conclusions …………………………………………………………….. 110

3.6 References ……………………………………………………………… 113

Chapter 4 Study the Gas Sensing Process of Nanoscale SnO_2 Thin Films by Fourier Transform Infrared Spectroscopy……………………………...118

4.1 Introduction…………………………………………………………….. 118

4.1.1 General Strategies in Study of Gas Sensing ……………………… 118

4.1.2 Theory of the Relations between Electrical Conductivity and IR Background Absorbance ………………………………………………120

4.2 Sample Preparation and Pretreatment……………………………….. 123

4.3 Oxygen Sensing Process……………………………………………… 128

4.4 CO Sensing Process …………………………………………………... 134

4.5 Is Oxygen Necessary for CO Detection? …………………………… 140

4.6 Dynamic Response of O_2 and CO Gas Sensing Process ……………..146

4.7 The Influence of Temperature on Gas Sensing Process ……………..147

4.8 Summary ………………………………………………………………. 152

4.9 References ……………………………………………………………… 154

Chapter 5 Thickness Effect on Sensitivity of Metal Oxide Semiconductor Gas Sensors ……………………………………………………………… 157

5.1 Introduction…………………………………………………………… 157

5.2 Experimental Details …………………………………………………. 159

PREVIEW

5.3 In-situ Monitor the SnO_2 ALD Process and the General Response to CO and O_2 by Electrical Measurements ……………………………………… 163

5.4 Thickness Effect on Sensitivity…………………………………………… 167

5.4.1 The First Approach: Using Single Hotplate Prototype Gas Sensor ……………………………………………………………………167

5.4.2 The Second Approach: Using Multiple Hotplate Prototype Gas Sensors ………………………………………………………………172

5.5 Temperature Effect on Gas Sensing Process ……………………………… 182

5.6 Summary ………………………………………………………………… 190

5.7 References ………………………………………………………………… 193

Chapter 6 Model of Gas Sensing Process on a Film with Thickness Close to the Debye Length ………………………………………………………………199

6.1 Model of Gas Sensing Process for Metal Oxide Semiconductor Gas Sensors with Thickness Close to the Debye Length ……………… 199

6.2 References ………………………………………………………………… 221

Chapter 7 Summary and Recommendations ………………………………… 223

7.1 Summary ………………………………………………………………… 223

7.2 Recommendations ………………………………………………………… 227

7.3 References ………………………………………………………………… 236

Bibliography ……………………………………………………………………237

PREVIEW

List of Tables

Table 1.1 Sample areas employing gas detection …….……………………….. 1

Table 1.2 Operation principles of solid-state gas sensors ……………………….. 3

Table 3.1 Precursors and temperatures used for SnO_2 atomic layer deposition and the results reported in literatures ………….....................……. 63

Table 3.2 Bond enthalpies involved in the half reactions during SnO_2 atomic layer deposition …….…………………………………………….…..... 71

Table 3.3 Fitting results of XRR for SnO_2 film deposited on silicon wafer by ALD at 275 °C 99

PREVIEW

List of Figures

Figure 1.1 Primitive tetragonal unit cell of the bulk rutile SnO_2 with the basis $(SnO_2)_2$ …… ………………………………………………………..………… 6

Figure 1.2 A model of stoichiometric SnO_2 (110) surface and the nomenclature for atomic positions ……….... …………..……….…..……...…….. 6

Figure 1.3 Schematic showing the point defect types on a simple crystal lattice... 7

Figure 1.4 Taguchi-type sensor element and packaged sensor ………….……..... 9

Figure 1.5 Schematic of typical thick film gas sensors ……………………..... 10

Figure 1.6 Micrograph of single micro-hotplate gas sensor and schematic of functional layers in this micro-hotplate gas sensor.………...…...….. 12

Figure 1.7 Micrograph of the integrated gas sensor and the packaging of the gas sensor ………...……………………...….……………........…..... 12

Figure 1.8 Schematic of depletion layer and potential barrier change at grain boundary ……………..…………………..…………………..…..... 15

Figure 1.9 Schematic band diagram of the SnO_2 bulk ……………………..…...... 16

Figure 1.10 Types of resistance contributions in a porous layer accounting for the grain size effects ……………..…...……………………………..... 19

Figure 1.11 Grain size influences on sensitivities of semiconductor gas sensors. 22

Figure 1.12 Schematic drawing of electrical model of compact thin films …..... 23

Figure 1.13 Schematic representation of atomic layer deposition using self terminating surface chemistry in an AB binary reaction sequence……. 26

Figure 1.14 Demonstration of excellent conformity and uniformity of ALD films………………………………………………………………….. 28

Figure 2.1 Schematic of Viscous Flow ALD Reactor System, Size not in scale . 52

Figure 2.2. Sample Mounting for FTIR Experiments. ………….……………….. 58

Figure 3.1. Linear growth of SnO_2 ALD films, mass gain during 20 $SnCl_4/H_2O_2$ AB cycles at 325 °C ………........…………………………..…..…… 68

Figure 3.2. Linear fit of the mass gains during 20 AB cycle SnO_2 ALD at 325 °C …………………………………………………………….....68

Figure 3.3. Mass gain after 20 AB cycles showing self-limiting of half reactions …………………………………………………………..70

PREVIEW

Figure 3.4. Enlargement of QCM mass changes and corresponding reactant pressure changes for two $SnCl_4$-H_2O_2 AB cycles during SnO_2 ALD at 325 °C. ………………………………………….…………….... 73

Figure 3.5. The dependence of hydroxyl coverage on temperature measure by FTIR using SnO_2 nanopowders …………………..……………..… 75

Figure 3.6. Mass gain after 20 $SnCl_4$-H_2O_2 AB cycles vs substrate temperature……………………………………………………………….. 78

Figure 3.7. IR spectrum of the initial surface of the substrate after pretreatment ……………………………………………………....... 81

Figure 3.8. Absolute FTIR spectra during the 1st AB cycle of SnO_2 ALD Process ………………………… ……………………………………...83

Figure 3.9. Difference spectra showing the infrared absorbance in the SnO-H stretching vibration region during the ninth and tenth $SnCl_4$-H_2O_2 AB cycles ...……….………………………………..……………..… 84

Figure 3.10. Absolute spectra referenced to the CsI windows from 400 to 4000 cm^{-1} showing the infrared absorbance after the H_2O_2 exposures vs number of SnCl4-H2O2 AB cycles at 325 °C. ……. 86

Figure 3.11: Infrared absorbance at 2500 cm^{-1} vs number of $SnCl_4$-H_2O_2 AB cycles at 325 °C shows the nucleation and linear growth period of SnO_2 ALD process……………………..………..…88

Figure 3.12: Infrared absorbance at 2500 cm^{-1} vs number of $SnCl_4$-H_2O_2 AB cycles at 325 °C ……….……..……………………...……89

Figure 3.13: Absolute spectra referenced to the CsI windows from 400 to 900 cm^{-1} showing the infrared absorbance after the H_2O_2 exposures vs number of $SnCl_4$-H_2O_2 AB cycles at 325 °C……….90

Figure 3.14: Infrared absorbance at 2500 cm^{-1} after each $SnCl_4$ and H_2O_2 exposure vs number of $SnCl_4$-H_2O_2 AB cycles at 325°C ...……..92

Figure 3.15: X-ray diffraction pattern of a SnO_2 thin film grown from 500 AB $SnCl_4$/H_2O_2 by using atomic layer deposition techniques ……..……96

Figure 3.16: X-ray diffraction patterns of SnO_2 thin films deposited on silicon wafers at various temperatures ………..…...…………..…..97

Figure 3.17: X-ray reflectivity curve from SnO_2 film deposited on silicon wafer at 275 °C …………………………………………………..…99

Figure 3.18: Auger electron spectra of SnO_2 thin film deposited on SiO_2/Si(100) substrate by ALD using $SnCl_4$/H_2O_2 as precursors ……………....101

PREVIEW

Figure 3.19: XPS spectra of SnO_2 thin film deposited on SiO_2/Si(100) substrate by ALD using $SnCl_4$/H_2O_2 as precursors ……..…..…….103

Figure 3.20: Voltage between probes changes with the current through the SnO_2 ALD thin film. ………..……….…………………...…….105

Figure 3.21: Resistivities of SnO_2 ALD films deposited by ALD at various temperatures ……...………………………………………..…106

Figure 3.22: 1 μm × 1μm 2-D AFM image of SnO_2 film growing from $SnCl_4$/H_2O_2 on SiO_2/Si(100) substrate at 350°C ………..…….……108

Figure 3.23: 1 μm × 1μm 3-D AFM image of SnO_2 film growing from $SnCl_4$/H_2O_2 on SiO_2/Si(100) substrate at 350°C ……………..….109

Figure 3.24: Evolution of rms surface roughness of SnO_2 thin films with the growth temperature ………………………………………..111

Figure 4.1 Absolute spectra referenced to the CsI windows from 400 to 4000 cm^{-1} showing the infrared absorbance after the $SnCl_4$ exposures vs number of $SnCl_4$-H_2O_2 AB cycles at 325 °C …………………. 126

Figure 4.2 Infrared absorbance at 2500 cm^{-1} vs number of $SnCl_4$-H_2O_2 AB cycles at 325 °C shows the nucleation and linear growth period of SnO_2 ALD process ……………………………….... 127

Figure 4.3 Absolute infrared spectra referenced to the CsI windows from 1200 to 4000 cm^{-1} showing the infrared absorbance change from freshly made SnO_2 thin films, heat pretreatment to CO and O_2 gas sensing process……………………………….……….... 129

Figure 4.4 Absolute spectra referenced to the CsI windows from 1200 to 4000 cm^{-1} showing the infrared absorbance after the O_2 exposures versus the oxygen pressure at 300°C. ……………………..…... 131

Figure 4.5 Infrared absorbance at 2500 cm^{-1} after the O_2 exposures versus the oxygen pressure at 300 °C. ………………………………... 132

Figure 4.6 Absolute spectra referenced to the CsI windows from 1200 to 4000 cm^{-1} showing the infrared absorbance after the CO exposures under O_2 circumstance versus the CO pressure at 300 °C (flow mode) …... 136

Figure 4.7 Infrared absorbance at 2500 cm^{-1} after the CO exposures under O_2 circumstance versus the CO pressure at 300 °C (flow mode) …. 137

Figure 4.8 Absolute spectra referenced to the CsI windows from 1200 to 4000 cm^{-1} showing the infrared absorbance after the CO exposures under O_2 circumstance versus time at 300 °C (static mode) …………..… 138

PREVIEW

Figure 4.9 Infrared absorbance at 2500 cm^{-1} after the CO exposures under O_2 circumstance, the pressure of O_2, CO and CO_2 versus time at 300 °C (static mode)………………………………………………… 139

Figure 4.10 Absolute spectra referenced to the CsI windows from 1200 to 4000 cm^{-1} showing the infrared absorbance versus the CO exposures without O_2 at 300 °C (flow mode)…………………… 142

Figure 4.11 Infrared absorbance at 2500 cm^{-1} after the CO exposures without O_2 versus the CO pressure at 300 °C (flow mode) ……... 143

Figure 4.12 Infrared absorbance at 2500 cm^{-1} under the CO exposures and evacuation versus time at 300 °C (flow mode) ……………. 145

Figure 4.13 Infrared absorbance at 2500 cm^{-1} under the O_2 exposures and evacuation versus time at 300 °C (flow mode) ………………. 148

Figure 4.14 Infrared absorbance at 2500 cm^{-1} under the CO exposures and evacuation versus time at 300 °C (flow mode, under O_2)……..... 149

Figure 4.15 Infrared absorbance at 2500 cm^{-1} under O_2 and CO versus temperature (flow mode) ……………………………………….. 151

Figure 5.1. Schematic of the feedthrough assembly for electrical measurements ……………………………………………………161

Figure 5.2. Resistance recorded during the SnO_2 ALD process carried out at 250 °C ………………………………………………………… 164

Figure 5.3. Resistance changes when exposed to O_2 and CO for a 60 AB SnO_2 ALD film at 325 °C ……………………………………………….. 165

Figure 5.4. Sensitivity at different oxygen concentrations for a 45 AB SnO_2 ALD film at 325 °C ……………………………………………… 168

Figure 5.5. Sensitivity at different CO concentration for a 45 AB SnO_2 ALD film with 53 m Torr O_2 flow at 325 °C ………………………… 169

Figure 5.6. Sensitivity versus CO concentration with film thicknesses ………. 170

Figure 5.7. Sensitivity versus number of AB cycles at 325 °C, base pressure of 0.76 torr with 55 mTorr O_2 and 150 ppm CO …………………… 171

Figure 5.8. Sensitivities of all prototype gas sensors change with CO partial pressure at 300 °C, The thicknesses of the films were listed on the right side ………………………………………………………. 174

Figure 5.9. The thickness effect on sensitivities …………………………… 175

PREVIEW

Figure 5.10: A schematic of the thin film and the equivalent circuit ...………177

Figure 5.11: A schematic of the thin film and the equivalent circuit …………..181

Figure 5.12: The sensitivity changes with the CO partial pressure under various sensing temperatures for a 2.6 nm thick prototype gas sensor…….184

Figure 5.13: Sensitivity change with sensing temperatures for 20 mTorr CO.…185

Figure 5.14: The kinetic response to 20 mTorr CO under various sensing temperature for a gas sensor with thickness of 26 Å ……………..187

Figure 5.15: The relation between the operation temperature and the thickness of the sensitive film that has the highest sensitivity ……………..…..189

Figure 6.1: Schematic of processes involved in the gas sensing process ………200

Figure 6.2: Schematic band diagram of the SnO_2 bulk …………...…………. 205

Figure 6.3: The relationship between sensitivity and film thickness ……..…. 220

Figure 7.1: Schematic of different effects of doping ……………………..…. 232

Figure 7.2: Double face planar and cylindrical structures adopted in manufacturing gas sensors to double the sensitivity ……….……..233

Figure 7.3: Schematic of coating conducive structures (particles, nanotubes, nanorods) to enhance the sensitivity of metal oxide semiconductor based gas sensors..……………………….……………………...235

PREVIEW

Chapter 1

Introduction and Literature Review

1.1 Overview of Gas Sensors

Gas detection plays an important role in our modern daily life; it has a variety of environmental, industrial, medical scientific and domestic applications. For example, detection of toxic and combustible gases is of great interest and required in fields like air quality control, combustion processes and engine emissions; quick and accurate gas detections are required for fire detection and localization. More applications of gas detection are listed in Table 1.1.

Table 1.1 Sample areas employing gas detection

Domestic Safety	**Air Quality Control**	**Automotive**
Gas and CO alarm Gas boiler safety switch Breath alcohol tester Humidity detector	Air purifier Air conditioner Ventilation control	Cabin air quality Air purifier LPG alarm for PV gas driven car
Appliance Control	**Industrial, Health & Safety**	**Aerospace & Airport**
Microwave oven Air purifier Cooker hood	Combustible gas detector Toxic gas detector Refrigerant leak detector Oxygen monitor	Combustible gas detector Explosive gas detector Drug detector

Gas detection methods can be split into two groups: (i) direct methods, which monitor a physical parameter of the target gas, and (ii) indirect methods, which use a chemical reaction or indicator to show the concentration of the gas being sensed [1]. Gas detectors can be classified into two categories according to their physical structures: solid-state gas detectors and non-solid state gas sensors.

PREVIEW

Based on the physical parameters of the target gas utilized, there are different types of non-solid-state gas detectors, such as gas chromatography and mass spectrometry. Also widely used are flame-ionization, photo-ionization and electron-capture gas chromatography detectors. These non-solid-state gas detectors often offer a direct, rapid, very accurate and highly selective means to measure the gas concentration with good sensitivity. However, the advantages of these instruments are partially offset by the disadvantage features. Non-solid-state gas detectors normally are complex, expensive, bulky and have higher requirements for gas sampling.

The disadvantages do not hold for solid-state gas sensor systems. Solid-state gas sensors normally have lower production costs, simple user procedures and high time and spatial resolution during detection. These are devices with lower detection range and versatility, which show better characteristics for routine analysis of specific chemicals or odors [2].

PREVIEW

1.2 Overview of Solid State Gas Sensors

Transducers are any device that can convert input energy of one form to output energy of another form for the purpose of measurement of a physical quantity or for information transfer [3, 4]. A gas sensor is a kind of transducer that detects gas molecules and produces an electrical signal with a magnitude proportional to the concentration of the gas [4]. The systematic production and characterization of new sensing materials, the availability of fast and sensitive electronic measuring systems, and the fast growing knowledge in information theory to analyze multidimensional complex data, make the development of solid-state gas sensors possible.

There are already commercial gas sensor devices used for identification of specific contaminants or common mixtures. Based on the different operation principles, a variety of solid state gas sensors have been developed, such as semiconductor, photothermal, optical and fiber-optic-based, piezoelectric, pyroelectric, and thermal devices. The operation principles of these solid-state gas sensors are shown in Table 1.2.

Table 1.2 Operation principles of solid-state gas sensors [5][6]

Sensor Types	Operation Principles
Semiconductor Sensors	Conductance changes with ambient gases
Photonic & Photoacoustic Gas Sensor	Optical constants of solid interface coupled with gases
Fiber-Optic Sensor	Light transmitted along an optical fiber modified by external chemical influences
Piezoelectric Quartz Crystal Microbalance Sensors	Gas pressure affects the vibration of coated quartz crystal microbalance
Surface Acoustic Wave Sensors	Interaction between surface acoustic wave surrounding media
Pyroelectric & Thermal Sensors	Shift of pyroelectric signal induced by the temperature change which was resulted from the gas adsorption energy

PREVIEW

Among all the solid-state gas sensor systems, semiconductor gas sensors are the most promising and play an important role in the detection of toxic pollutants (CO, H_2S, NO_x, SO_2 etc.) and inflammable gases (H_2, CH_4, hydrocarbons etc.), due to their small size, low cost, and simple operation [7-8]. The first commercial metal oxide semiconductor gas sensor was developed by Tagushi [9] in the 60s, not long after the work of Seiyama [10], who

applied the effect of the ambient atmosphere upon the electrical conductance of semiconductors to gas detection. Currently, metal oxide semiconductor sensors comprise a significant part of the gas sensor component market, which is projected to exceed 2.5 billion dollars by 2010 [11].

Metal oxide semiconductor layers used for gas detections undergo conductance changes under the influence of ambient gases. The interaction mechanisms between the gas phase and the sensing material involve mainly physisorption, chemisorption, surface defects, bulk defects or three phase boundary processes. Physisorption is maintained by the weak van der Waals forces and has an undselective character; Therefore, sensors based on physisorption processes usually exhibit sensitivity to a wide range of gaseous species. On the other hand, chemisorption is a stronger interaction, and sensors based on chemisorption show a higher selectivity. Chemisorption is usually promoted by surface defects. The chemical bonds formed from adsorbates and the surface atoms modify the electronic structure of both the adsorbate and the surface. The conductance change may take place either on the surface or in the bulk. Surface conductance changes are usually associated with electron transport processes, while bulk conductance changes generally imply ion transport [6].

Numerous materials have been reported to be used as metal oxide sensors, including both single-component (e.g., ZnO, SnO_2, WO_3, TiO_2, Fe_2O_3 and Ga_2O_3) and multi-component oxides ($BiFeO_3$, $MgAl_2O_4$, $SrTiO_3$, and Sr_{1-y} Ca_yFeO_{3-x}). More metal oxide semiconductor materials examined for gas sensing purposes are listed in Table 1 in reference [12-13]. The example materials using surface-conductance and bulk-conductance were shown in

PREVIEW

Table 1 of reference [14]. Among them, n-type SnO_2 is a popular sensor material and has been widely investigated, because of its relatively high sensitivity, low cost, fast response, low power consumption and good chemical stability [12, 15].

1.3 Tin Oxide Based Metal Oxide Semiconductor Gas Sensors

1.3.1 Crystal Structure and Properties of Tin Oxide

Tin oxide is an n-type semiconductor with a wide optical band gap of 3.6 eV. Tin oxide has many applications in various fields due to its special optical, electrical and chemical properties. Many of these properties result from the ability of SnO_2 to form oxygen vacancies, dislocations or interstitial atoms that produce electron charge carriers. For example, its high conductivity when doped, together with its transparency makes SnO_2 an ideal material for producing transparent electrodes, which are widely used in flat panel displays and solar cells [16-17]. SnO_2 is a promising high capacity anode for next generation lithium ion batteries [18-19]. SnO_2 can also be used as a catalyst for oxidation of CO, CH_4 and the other organic molecules [20-21]. A huge effort has been made in empirical optimization of this material by varying the type of dopants, amount of doping, sintering conditions, grain size, and operating temperature.

PREVIEW

Tin oxide crystallizes in only one stable phase, which has a tetragonal arrangement of the atoms receiving the names of rutile or cassiterite, similar to TiO_2, CeO_2 or GeO_2 [22]. The unit cell of this crystalline structure contains two tin and four oxygen atoms, with the tin atoms in octahedral coordination and oxygen atoms in planar three-coordination (see Figure 1.1) [23-24]. The lattice parameters for this structure are a = 4.737 Å (a=b in the tetragonal

structure) and c = 3.186 Å. In SnO_2, chemical bonding is mainly governed by the linear combination of oxygen 2s and 2p orbitals with tin 5s and 5p orbitals [25]. The corresponding heat of formation is $\Delta H = 1.9 \times 10^3$ J mol^{-1}. Tin oxide has a heat capacity of Cp = 52.59 J mol^{-1} K^{-1} , a density of 6.95 g cm^{-3} at 300K and the melting point is 1630 °C.

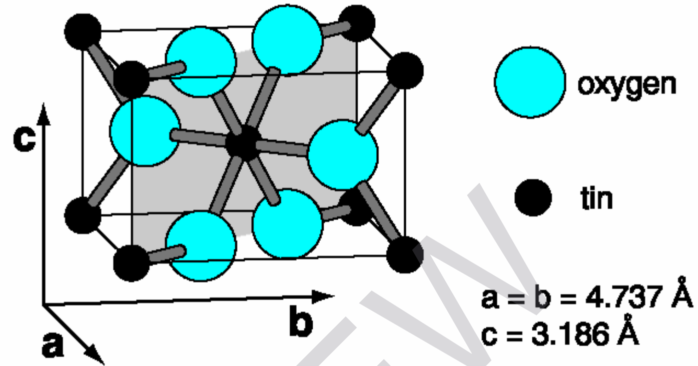

Figure 1.1: Primitive tetragonal unit cell of the bulk rutile SnO_2 with the basis $(SnO_2)_2$. The bigger circles represent oxygen atoms. The shaded area represents the (110) cleavage plane [23-24]

PREVIEW

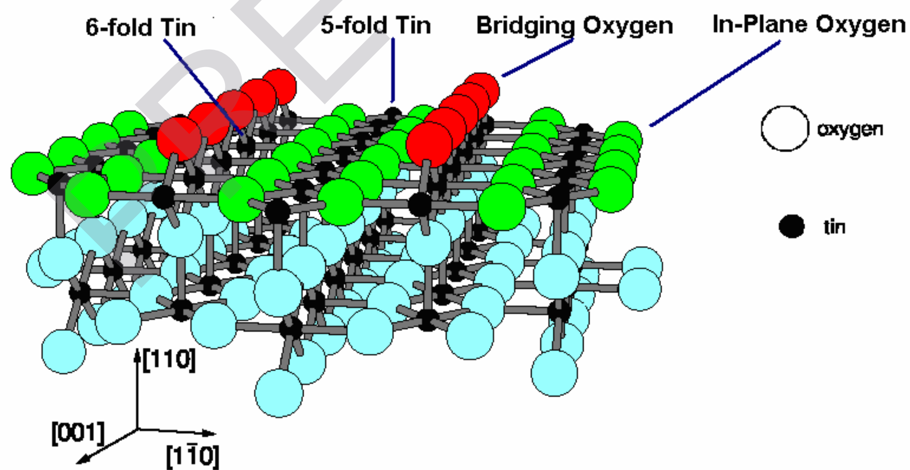

Figure 1.2: A model of stoichiometric SnO_2 (110) surface and the nomenclature for atomic positions. Bigger circles represent oxygen atoms [26]

The single crystal SnO_2 (110) surface, which is the thermodynamically most stable surface space [26], is the predominant termination of SnO_2 on both the macroscopic crystals and nanoscopic particles [27]. This surface has been paid wide attention as a model system for SnO_2 gas sensors and catalysis.

A stoichiometric surface is illustrated by Figure 1.2, where the bridging oxygen rows are complete. The atoms on the crystal surface usually arrange themselves and result in quite different electronic states from the bulk. Given the incomplete coordination, the surface shows an increased reactivity towards the colliding particles.

A defect is any region where the microscopic arrangement of the particles differs from a perfect crystal. These may be called surface or bulk defects according to whether the imperfect region is on the surface or in the bulk. The types of bulk defects are schematically shown in Figure 1.3 [3]. The most frequent intrinsic surface defect in the n-type semiconducting oxides (SnO_2) is a donor-type oxygen vacancy. The stoichiometric surface of SnO_2 (110) will loose its bridging oxygen after heating to 700 K. Further heating removes in-plane oxygen, and leads to an increased defect density [28-30]. On the surface, both line and point defects are important to gas sensing processes. Other surface defects important in the gas sensing mechanisms are impurities or dopants. Their electronic and geometric influence on sensor properties is usually correlated with catalytic properties [31].

PREVIEW

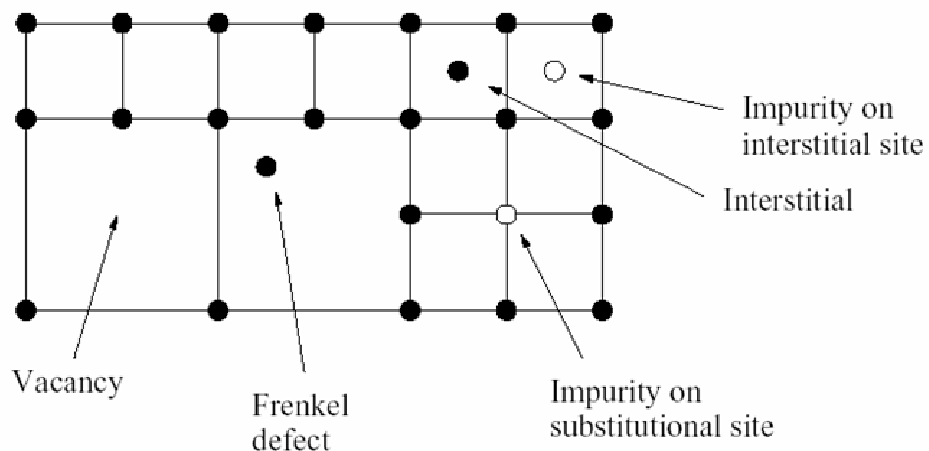

Figure 1.3: Schematic showing the point defect types on a simple crystal lattice